ELSEVIER

Thermochimica Acta 388 (2002) 199–213

thermochimica acta

www.elsevier.com/locate/tca

Measurement and modeling of individual carbonaceous particle temperature profiles during fast CO_2 laser heating Part 2. Coals

Ashish Tripathi[a], Chris L. Vaughn[a], Waleed Maswadeh[b], Henk L.C. Meuzelaar[a,*]

[a]*Center for Microanalysis and Reaction Chemistry, The University of Utah, Salt Lake City, UT 84112, USA*
[b]*Geo-Centers, E3220 Aberdeen Proving Grounds, Aberdeen, MD 21010, USA*

Received 28 June 2001; received in revised form 4 October 2001; accepted 4 October 2001

Abstract

In part 1, we discussed the temperature profiles of laser heated spherical carbonaceous particles along with the temperature modeling. In this paper, we perform the same set of experiments with selected coal particles. Coals of three different ranks (i.e. degree of coalification) represented by three different particle sizes (80, 100, and 120 μm), with and without aerodynamic size classification, were analyzed under the same set of experimental conditions. The temperature profiles were modeled using a heat transport model modified to include chemical kinetics (based on the FG-DVC model). Non-aerodynamically size-classified particles displayed better model prediction when laser heated in nitrogen atmosphere compared with heating in air. Best model predictions, however, were obtained in the case of aerodynamically size-classified particles heated under nitrogen atmosphere.

Keywords: Carbonaceous particles; Non-aerodynamically; Devolatilization

1. Introduction

Obtaining reliable temperature data is one of the most important requisites for any chemical kinetics study. In the coal devolatilization kinetics literature there are large discrepancies in the reported values of activation energies and frequency factors [1,2] due to many reasons, one of the important reason is the lack of reliable temperature measurements. Reliable temperature measurement becomes even more challenging under pulverized coal combustion (PCC) conditions which are characterized by rapid heating rates (in the order of 10^5 K/s), high final temperatures (typically 1500–2000 K) and particle sizes up to 100 μm [3]. To study the devolatilization behavior of single coal particles in the PCC conditions, a laser pyrolysis system was constructed described elsewhere [4,5]. This system was shown in part 1 to be capable of heating single carbonaceous particles in the 80–120 μm size range, at heating rates in excess of 10^5 K/s while simultaneously recording the temperature histories. It is imperative to understand the system operating envelope, i.e. particle size range, laser power setting and two-color pyrometry limits, as well as the effects of coal type and rank. One also needs to investigate whether particle surface temperature measurements are relevant for studying devolatilization kinetics. Earlier reports [6,7] indicate that marked

* Corresponding author.
E-mail address: meuzelaar@mail.marc.utah.edu (H.L.C. Meuzelaar).

0040-6031/02/$ – see front matter
PII: S0040-6031(02)00030-8

intraparticle gradients may exist thus resulting in erroneous kinetics calculations. To investigate the relevance of these phenomena for our experimental conditions, a heat transport model incorporating chemical kinetics considerations was written.

Particles of different size representing three coals of different rank, namely Upper Freeport (medium volatile bituminous), Illinois #6 (high volatile C bituminous) and Beulah Zap (lignite) were obtained from the Argonne Premium Coal Sample program. These particles are not aerodynamically sized. These coal particles were irradiated by a CO_2 laser and their surface temperature histories measured. The surface temperature histories were then modeled with the aid of modeling techniques described by other researchers [6–16] but specially modified for our needs and modified to included chemical kinetics dependencies. Effect of aerodynamic size classification was also studied.

2. Experimental

The experimental setup is described in detail in part 1 of this two part article.

2.1. Sample preparation

Upper Freeport (coal ID #101, batch #02230), Illinois #6 (coal ID #301, batch #00099) and Beulah Zap lignite (coal ID #801, batch #00143) coals from the Argonne Premium Coal Sample Program (APCSP) [17] were sieved to obtain $-120 + 170$ mesh fractions. Single particles in this size range were used.

2.2. Experimental procedure

Individual coal particles of 80, 100, and 120 μm average sizes are hand-picked with a clean stainless steel needle under a stereo microscope (100× magnification) and carefully deposited onto an electron microscopy grid with 45 μm × 45 μm square holes separated by 5 μm thick bars. The size of each particle is measured by a careful visual comparison against the grid spacing. The particle on the EM grid is placed at the point of intersection of the two laser beams (the point of intersection is determined with the help of HeNe laser guide beams). The particle is then irradiated by a 25 or 30 ms laser pulse, while simultaneously the surface temperature history of the heated particle is measured by the two-color pyrometer. For each case (i.e. particle size and rank) at least four individual particles are irradiated with the laser to account for particle to particle variability.

3. Heat transport model

The heat transport model described in part 1 was modified to incorporate physical and chemical changes encountered by the devolatilizing coal particle. The modification on the assumptions and equations are described in the following paragraphs.

3.1. Assumptions

Following are the simplifying assumptions:

Assumption 1. All particles are perfectly spherical in shape.

This assumption allows the use of spherical coordinates and also permits the generation of easily defined boundary conditions. Since coal particles are rarely, if ever, spherical in shape, a sphericity correction factor must be used to correct for their non-spherical shape. We used the largest particle dimension to represent the size of the particle and hence the diameter of a sphere of the same volume is less than the size of the particle. Therefore, we define the sphericity correction factor as the ratio of the diameter of a volume equivalent sphere to the largest dimension of the particle. A sphericity correction factor of 0.75 was applied to all the APCSP coal particles irrespective of coal rank or particle size.

Assumption 2. Particles are porous.

As coal devolatilizes, the volatiles evolve from inside of the particle to the surface and escape. This causes a disruption in the boundary layer requiring a correction for the convective heat transfer coefficient, which is achieved by blowing factor analysis. This approach was used by Fletcher [9]. The internal heat transport due to flow of volatiles was not considered because of the complexity of the process and the lack of literature data support.

Assumption 3. The laser beams irradiate the particle from all the sides.

This assumption is the same as the one used in part 1.

Assumption 4. Coal changes to char.

As the devolatilization proceeds coal changes to char and this translates into an accompanying change of thermophysical properties from those of coal (0% conversion) to those of char (100% conversion). The thermophysical properties of devolatilizing coal are the conversion weighted average of those of the initial coal and final char.

Assumption 5. FG-DVC model used to predict coal kinetics.

For the thermophysical properties to be conversion dependent and also to have a heat of reaction term in the governing model equation, it is imperative to know the conversion history of the devolatilizing coal particle. Though there are many models to obtain conversion data for coal, we have used the FG-DVC model based on average temperature histories. This procedure will be discussed in a later section.

3.2. Model equations

The basic model equations are explained in the part 1 of this two-part article. In this section, the differences that are introduced due to the changed assumption, which incorporate the chemical kinetics aspects of coal heating, will be discussed.

Statement (a), (b) and (c) from part 1 of the article are applicable similarly in addressing the coal heating, but with one difference. The convective heat transfer coefficient 'h' is corrected to incorporate the effect of volatile blow through the surface of the devolatilizing coal particle. Therefore, Eqs. (1) and (3) remain unchanged while Eqs. (2), (4) and (5) are changed to:

$$Q_{\text{convection}} = h_{\text{BF}}(T_{\text{s}} - T_{\text{a}}) \tag{2}$$

where, 'h_{BF}' is the convective heat transfer coefficient with blow factor correction

$$Q_{\text{out}} = h_{\text{BF}}(T_{\text{s}} - T_{\text{a}}) + \sigma\varepsilon(T_{\text{s}}^4 - T_{\text{a}}^4) \tag{4}$$

$$K_{\text{c}}\left(\frac{\partial T}{\partial r}\right)_{\text{at } r=R} = I_0 a - \{h_{\text{BF}}(T_{\text{s}} - T_{\text{a}}) + \sigma\varepsilon(T_{\text{s}}^4 - T_{\text{a}}^4)\} \tag{5}$$

Eq. (5) becomes a boundary condition at the surface of the particle, i.e. Eq. (5) holds true at $r = R$.

To determine the heat transfer coefficient, h, we selected the approach outlined by Bird et al. [18], which is described in Eqs. (6a), (6b) and (7) of the part 1 and corrected the heat transfer coefficient with the blow factor analysis used by Fletcher [9] to obtain h_{BF}:

$$h_{\text{BF}} = \frac{hB}{(\mathrm{e}^B - 1)} \tag{7a}$$

where 'B' is the blow parameter defined by:

$$B = C_{\text{g}}\frac{(\partial m_{\text{c}}/\partial t)}{(2\pi D_{\text{p}} K_{\text{g}})} \tag{7b}$$

where 'C_{g}' is the specific heat capacity of the surrounding gas and 'm_{c}' is the mass of the particle.

Thermophysical properties of the surrounding gas (here air) are obtained from the literature [19,20]. The thermophysical properties of the surrounding gas are determined at the average temperature of the particle surface and the surrounding gas.

Statement (d). At the center of the particle, the temperature and conversion gradient are zero.

That is:

$$\left(\frac{\partial T}{\partial r}\right)_{r=0} = 0 \tag{8a}$$

$$\left(\frac{\partial X}{\partial r}\right)_{r=0} = 0 \tag{8b}$$

where 'X' is the conversion.Eqs. (8a) and (8b) are the boundary conditions at $r = 0$.

Statement (e). Before the laser is fired, the particle is at thermal equilibrium with the surrounding atmosphere and the coal particle is yet to undergo devolatilization.

That is:

$$T = T_{\text{a}} \tag{9a}$$

$$X = 0 \tag{9b}$$

$$\rho_{\text{c}} = \rho_{\text{c}_0} \tag{9c}$$

Eqs. (9a)–(9c) are the initial conditions.

Statement (f). An energy balance applied over a finite element volume results in the following

governing equation:

$$\frac{\rho_c C_c \partial T}{\partial t} = \frac{1}{r^2}\frac{\partial(r^2 K_c \partial T/\partial r)}{\partial r} + \frac{\Delta H_{rx}\partial(\rho_c X)}{\partial t} \quad (10)$$

where, 'ρ_c', 'C_c', 'K_c' and 'ΔH_{rx}' are the density, specific heat capacity, thermal conductivity and heat of the reaction of the coal particle respectively. The heat of reaction of the coal particle can be due to the conversion of the coal to light gases, tar, char and any other series or parallel reactions that could occur due to the coal devolatilization process. A detailed addressing of these reactions is beyond the scope of this article.

Eq. (10) is the governing partial differential equation, subject to boundary conditions described by Eq. (5) and (8) and initial condition described by Eq. (9).

3.3. Thermophysical properties

All the thermophysical properties discussed below are in SI units. Thermophysical property data for coal are available for specifically slow heating regimes [17,21,22] and the compositional change of devolatilizing coal adds further variability to these properties. Work done by Merrick [23–25] can give reasonable estimates of specific heat capacity, density and thermal conductivity data, if the devolatilization kinetics and the changes in coal composition are known.

3.3.1. Specific heat capacity of coal

The specific heat capacity of coal can be estimated with Merrick's model [23]. To use this model, the elemental composition and ash content of the coal must be known. The elemental composition is predicted by the FG-DVC model [26]. The model was used to predict the final elemental composition of coal after devolatilization. It was assumed that elemental composition functionality of coal (as used by Merrick's model) changes linearly with coal conversion.

$$C_c = C_{af}(1 - X_{ash}) + C_{ash}X_{ash} \quad (11a)$$

where 'C_{af}' is the specific heat capacity of the ash free coal, 'C_{ash}' ($C_{ash} = 754 + 0.586T$) is the specific heat capacity of the ash, 'X_{ash}' is the fraction of ash in coal.

$$C_{af} = (1 - X)C_{c_0} + XC_{char}$$

where, $C_i = R/a_i[G(\theta_1/T) + 2G(\theta_2/T)]$, $i = c_0$ or char and $G(z)$ is a function defined as: $G(z) = z^2e^2/(e^z - 1)^2$; $1/a_i = \sum_{j=1}^{5} y_j/M_j$, where y and M are the mass fraction and atomic weights of carbon, hydrogen, oxygen, nitrogen and sulfur, respectively. This information is given in Table 1. The temperature dependent specific heat capacities of initial coal and final char are evaluated from elemental composition predictions obtained from FG-DVC model.

3.3.2. Density of coal

The initial density of coal is assumed to be 1300 kg/m^3. The final density of coal (in char form) is calculated by the total weight loss of coal particles during devolatilization. The instantaneous density of coal is the conversion weighted average of the initial and final coal density [24]:

$$\rho_c = \frac{\rho_{c_0}}{[1 - X(\rho_{c_0}/\rho_{char})]} \quad (11b)$$

where, $\rho_{char} = \rho_{c_0}X_{wt.\ loss\ frac}(1 - X_{ash})$, ρ_{c_0} is the initial coal density and $X_{wt.\ loss\ fract}$ is the fraction weight lost. Size of the particle is assumed to remain constant

Table 1
Information on coal

Coal	Upper Freeport		Illinois #6		Beulah Zap	
	Initial	Final	Initial	Final	Initial	Final
Weight present, daf (based on FG-DVC model)	100	54.7	100	45.6	100	58.2
Carbon (%)	85.60	96.24	77.70	93.79	73.00	97.10
Hydrogen (%)	4.70	1.01	5.00	1.04	4.80	1.5
Oxygen (%)	7.40	0.33	13.70	0.67	21.50	0.71
Nitrogen (%)	1.50	1.42	1.40	1.43	0.7	0.65
Sulfur (%)	0.80	1.00	2.20	0.800	0.00	0.00
1/a (used by Merrick's model for sp. ht. capacity)	0.1293	0.0918	0.1250	0.0910	0.1228	0.0972
Ash fraction	0.13	0.13	0.16	0.16	0.06	0.06
Weight loss based on FG-DVC model, dry basis percentage	39.5	39.5	45.7	45.7	38.9	38.9

during devolatilization (Assumption 1). Table 1 displays the weight loss data.

3.3.3. Thermal conductivity of coal

The thermal conductivity of coal can be estimated with Merrick's model [25]. This model uses "true solid density" of coal to determine the thermal conductivity of coal. It is assumed that true solid density of coal is 1600 kg/m^3 and it remains constant through out the devolatilization process (only apparent particle density changes).

$$K_c(T) = 0.02685T^{1/2} \quad (11c)$$

Though the true solid density of the particle will increase as the devolatilization proceeds because of the increase in the carbon content of the devolatilizing coal. The result of the increase in true solid density is increase in the thermal conductivity of coal, which should reduce the intraparticle temperature gradient, thereby reducing the risk of using the surface temperature in kinetics calculations. Moreover, the sensitivity analysis performed on the affect of thermal conductivity shows that surface temperatures are largely unaffected by changes in thermal conductivity. Therefore, it is safer to underestimate the value of thermal conductivity of coal as it would provide for a

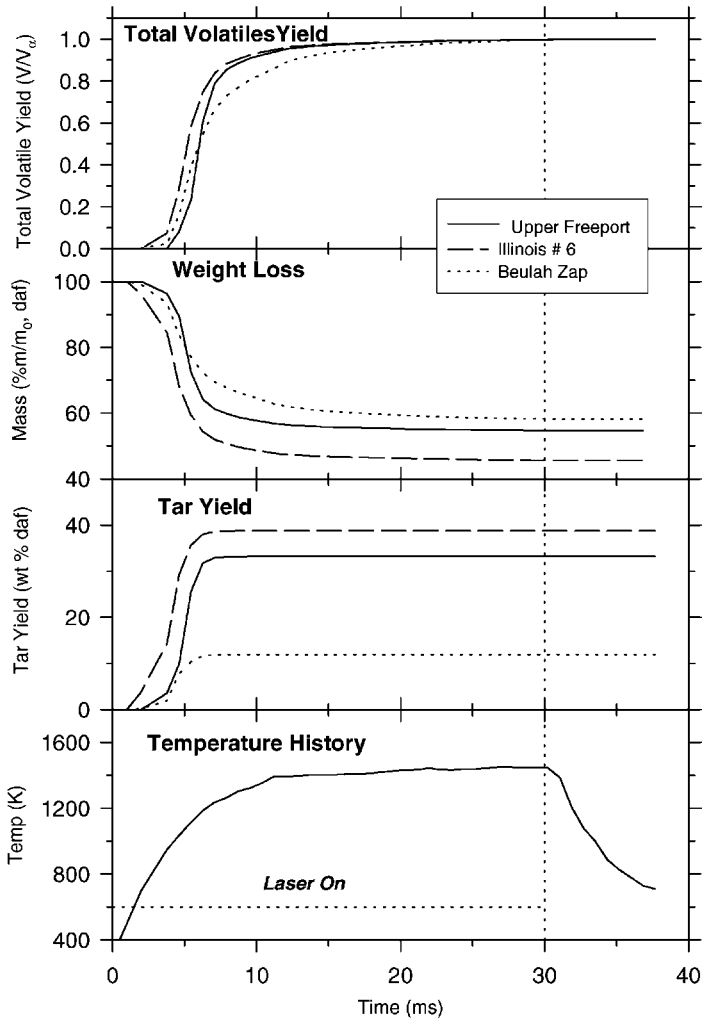

Fig. 1. FG-DVC model predictions using the temperature history shown.

safer estimates of the bulk average temperatures and hence the true solid density of coal is assumed to be 1600 kg/m^3 (lower value).

3.3.4. Thermophysical properties of surrounding gas

These experiments were done in an ambient air atmosphere. Thermophysical properties of air used [19,20] are described in Table 1 of part 1 of this article.

3.4. Coal devolatilization kinetics

Since the thermophysical properties are conversion dependent and further the heat of reaction terms appear in the governing equation (Eq. (10)), the thermophysical properties are coupled to predictions of coal conversion. A further requirement is to know the elemental composition of coal during the devolatilization. This can be estimated by means of the FG-DVC model [26]. A simpler approach would be the use of the DAE model [27] but this model does not provide elemental composition information. Fig. 1 shows the temperature history used for the three coals and the FG-DVC results showing the weight loss and yield curves.

3.5. Sphericity of coal

Coal particles are non-spherical. This requires a "sphericity factor" [28]. Further adding to this complexity the APCSP coals are not aerodynamically sized. To do so, ourselves would result in the introduction of new sources of variance, thereby negating our attempt to utilize the advantage of using standard coal samples. Thus, highly irregularly shaped particles can be expected to be present (i.e. two of the three dimensions could be much larger than the third one). Monozam and Maloney [28] have emphasized that coal particles sized by conventional screen sieving methods could have sphericity factors (defined as the surface area of a volume equivalent sphere divided by the actual surface area) as low as 0.73, while sphericity factors for aerodynamic size classification could be as high as 0.89. Since our experiments were conducted on screen-sieved coal particles, we have assumed a sphericity correction factor of 0.75.

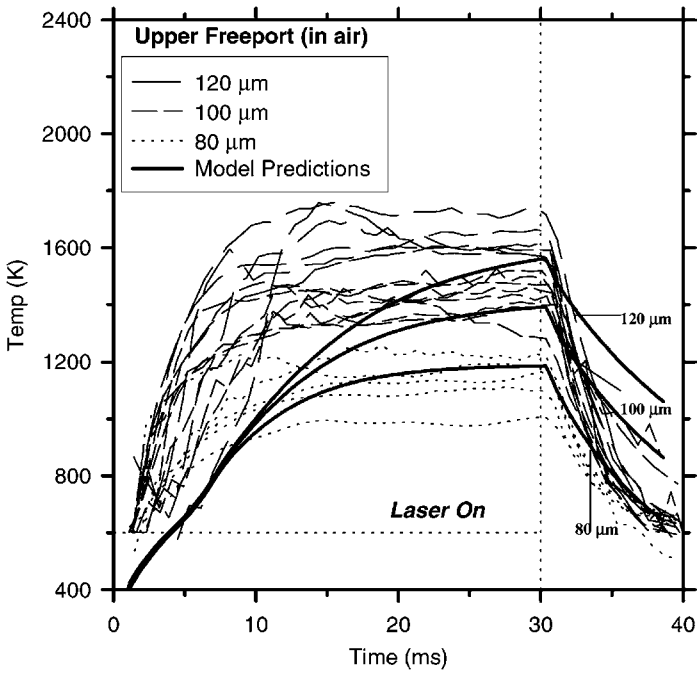

Fig. 2. Surface temperature histories of 80, 100, and 120 μm Upper Freeport coal particles and model predictions in air atmosphere.

4. Results and discussion

4.1. Upper Freeport coal particles

Small sets (6–9 particles) of single 80, 100, and 120 μm sized Upper Freeport coal particles were individually irradiated with a 30 ms long CO_2 laser pulse at ca. 10 MW/m^2 in ambient air and their surface temperature histories measured. Measured particle surface temperature histories were modeled, using only the absorbed laser flux as a fit parameter (1.68, 1.96, and 2.24 MW/m^2 for 80, 100, and 120 μm sizes, respectively). The modeling results along with the particle surface temperature histories are shown in Fig. 2. Fig. 3 illustrates the particle surface physical property histories predicted by the model. The model predicts a slower heating rate initially, owing to the predicted rapid increase in the specific heat capacity in the first 5 ms. It was also observed that in the case of 100 and 120 μm sized particles the plateau temperature was not reached within the 30 ms heating period. However, the plateau temperature was attained in the case of 80 μm particles. Also, the model predicts much slower cool-down rates than observed in the case of 100 and 120 μm sized particles. In essence, it was found that larger particle heat-up and cool-down much faster than the model predicts. These discrepancies will be addressed later.

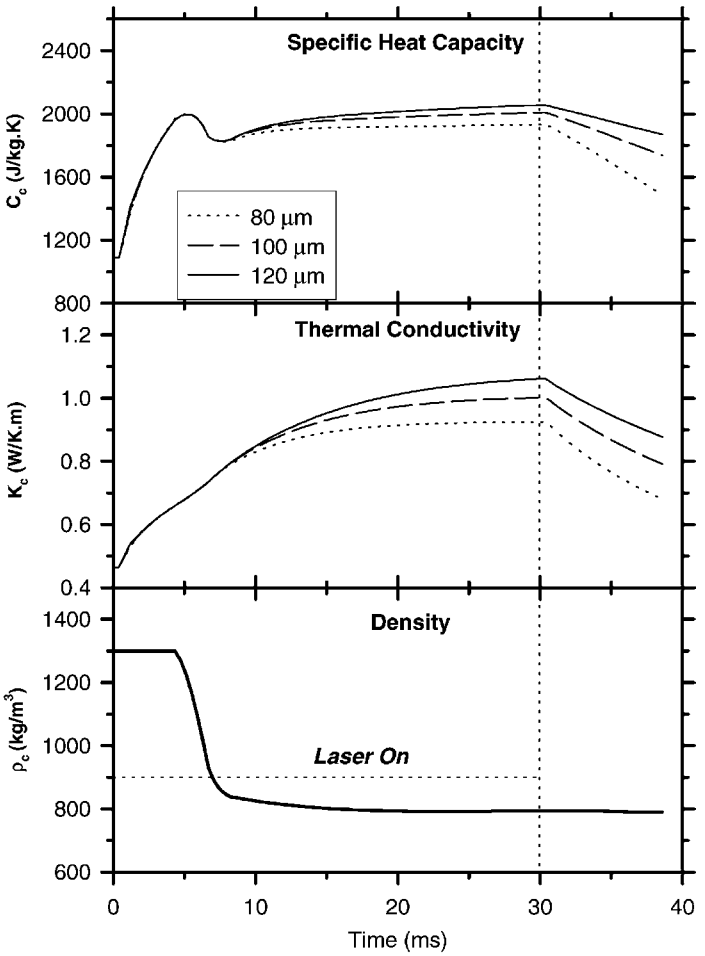

Fig. 3. Predicted surface thermophysical property histories of the three sizes of Upper Freeport coal particles.

4.2. Illinois #6 coal particles

Individual, 80 and 100 μm sized coal particles were irradiated with a 25 ms long laser pulse. These experiments were performed at the same laser power setting as the Upper Freeport coals and in ambient air atmosphere. The laser power absorbed by the particle was same as that for Upper Freeport coals of corresponding size. Again the model predicts similar initial heat-up behavior as that predicted for Upper Freeport coal and slower initial heating rates than observed. Also note that, for 100 μm particles, there is an apparent "overshoot" of measured temperatures (or under-prediction by the model) following initial heat-up. The plateau temperatures reached by 100 μm particles are approximately was not attained by the model prediction in 25 ms heating. This observation will be discussed in following paragraphs. Also the cool-down rates predicted by the model are lower than those observed. We also tried to measure the temperature histories of 120 μm sized particles, but it was hard to keep the particles stationary on the grid during irradiation. Furthermore, the initial temperature "overshoot" was found to be hundreds of Kelvin for these large particles. Fig. 4 shows the modeling results for 80 (using 1.68 MW/m^2 as absorbed laser power) and 100 μm (using 1.96 MW/m^2 as absorbed laser power) Illinois #6 particles along with the measured particle surface temperature histories. Fig. 5 shows the particle surface physical property histories predicted by the model.

4.3. Beulah Zap coal particles

Individual 80 μm sized coal particles were irradiated with a 30 ms laser pulse. The laser power setting was the same as that used for Upper Freeport and Illinois #6 coals. The experiments were done in ambient air. The measured particle surface temperature histories (of 12 single particles) and the heat transport model predictions are shown in Fig. 6. It is observed that measured heating rates in the first 15 ms are higher than predicted by the model. This is similar to the initial temperature "overshoot" observed in the laser heating of 100 μm Illinois #6 particles (in ambient air). Again, the cool-down rates predicted by the model were much slower than those observed. We tried obtaining the temperature histories

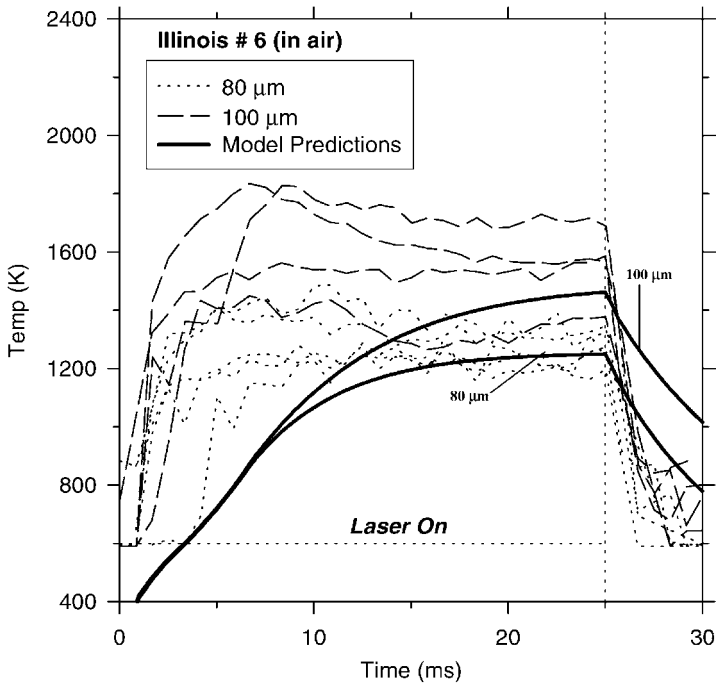

Fig. 4. Measured and predicted surface temperature histories of 80 and 100 μm Illinois #6 coals particles pyrolyzed in air atmosphere.

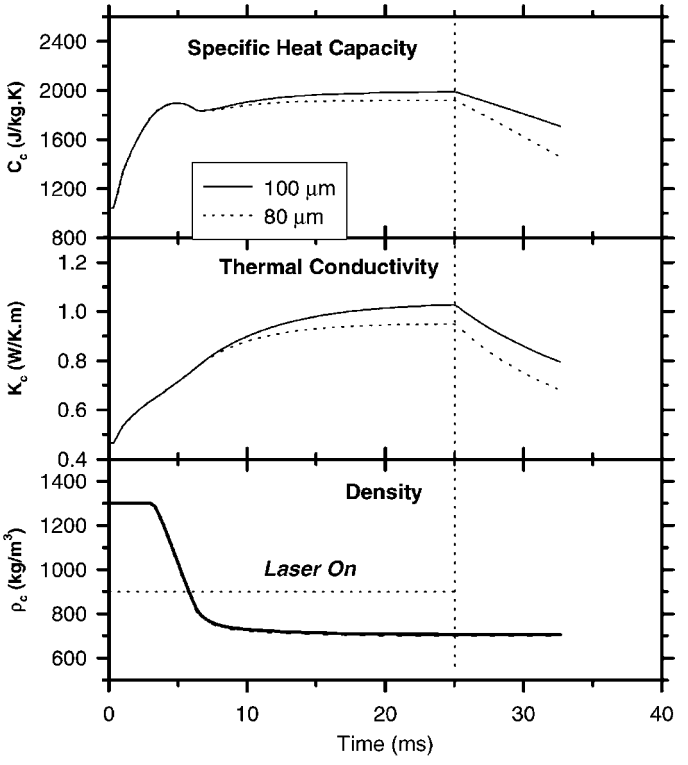

Fig. 5. Predicted surface thermophysical property histories of the two sizes of Illinois #6 coal particles.

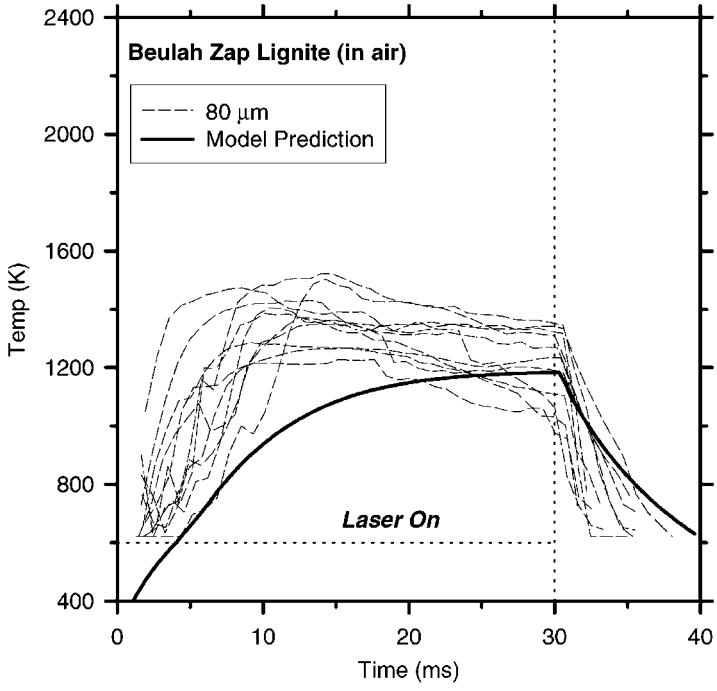

Fig. 6. Measured and predicted surface temperature histories of 80 μm Beulah Zap lignite particles pyrolyzed in air atmosphere.

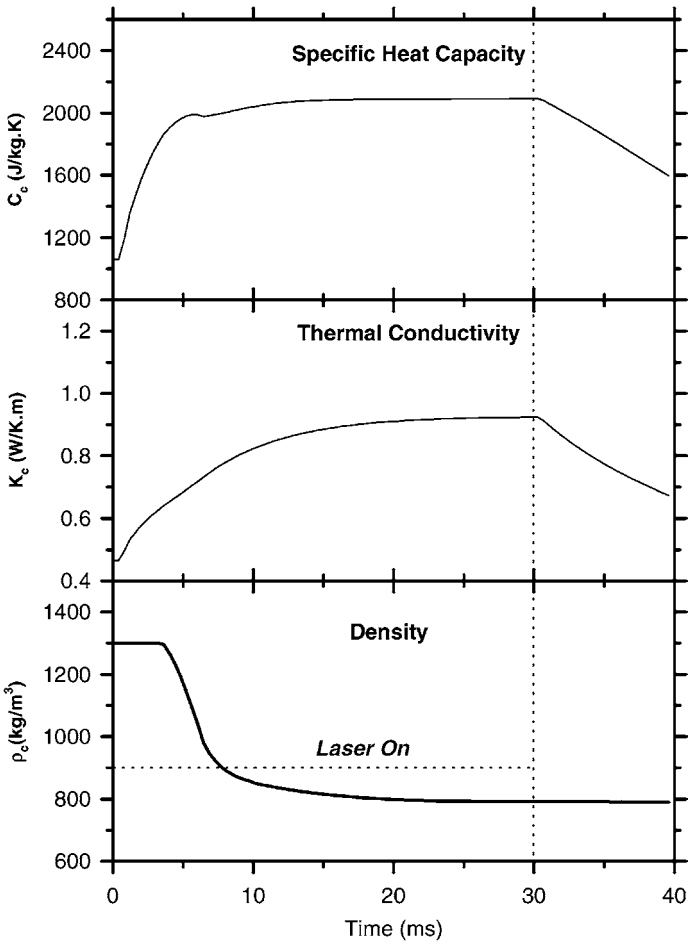

Fig. 7. Predicted surface thermophysical property histories of 80 μm Beulah Zap lignite particles.

of larger (100 and 120 μm) particles but were hindered by our inability to keep the particle stationary and in the few instances where we could keep the particle stationary, initial temperature overshoots of several hundred degrees Kelvin were observed. Fig. 7 shows the predicted thermophysical property histories of the particle surface.

4.4. Exothermic effects

The observed initial "overshoot" of the temperatures (as seen in Figs. 2, 4 and 6) in comparison to those predicted by the model increased with increasing particle sizes and decreasing coal rank. An obvious explanation for this discrepancy could be the exothermic combustion of evolved tar and gas products. Larger particles have higher volume to surface area ratios. This means that each unit area of external surface receives a larger volume of devolatilization products, hence increasing the probability of the oxidation of these products in the vicinity of the particle surface (which is in contact with ambient air). Also in case of the lower rank coals which produce more light gases than tar (which is highly labile [29]), increasing the probability of volatile combustion, added to that, low rank coal char is highly oxidative and hence more likely to heterogeneously combust. Though the exact mechanism of oxidation (i.e. to say volatile or char oxidation or combination of both) cannot be commented upon, nevertheless the presence of oxygen could

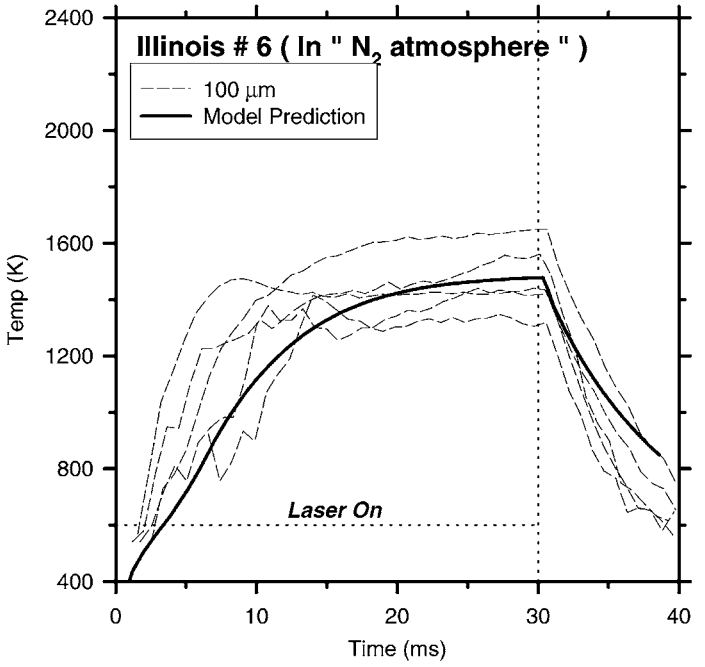

Fig. 8. Measured and predicted surface temperature histories of 100 μm Illinois #6 coal particles pyrolyzed by laser under a nitrogen atmosphere.

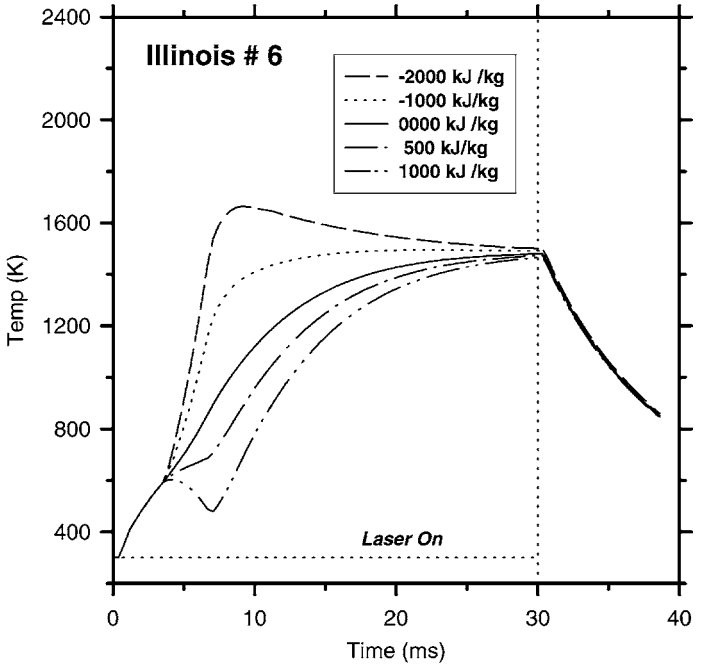

Fig. 9. Predicted effect of heat of reaction on the surface temperature history of a 100 μm Illinois #6 coal particle.

well be responsible for the observed overshoot. This hypothesis prompted us to heat 100 μm Illinois #6 particles in a ''nitrogen atmosphere''. Fig. 8 shows the temperature histories of four 100 μm sized Illinois #6 particles and the modeling results, using the same laser power as used for 100 μm Illinois #6 particles in air. As can be seen, the model agrees better with the measured heating up, as well as cool down behavior. We ran modeling prediction scenarios using various heats of reaction. These results are shown in Fig. 9. The predicted initial delays in the start of heat-up can be attributed to the rapid initial increase in the specific heat capacity (as seen in Figs. 3, 5 and 7), which results in heat storage without apparent increase in temperature.

4.5. Intraparticle temperature gradients

The model was used to predict the temperature gradients existing in 120 μm particles of the three coal ranks. The difference between bulk average temperature and surface temperature never exceeds 100 K. This temperature difference is less than the measured temperature variations from particle to particle, which exceeds 300 K in most cases. Though these gradients are at their maximum when the reaction rates reach a maximum (as predicted by the FG-DVC model), they can still be ignored as long as a statistically valid set of temperature histories are obtained. Fig. 10 shows the temperature gradients existing in these particles.

4.6. Effect of aerodynamic size classification

Aerodynamically size-classified coal samples were obtained through the courtesy of Dr L. L. Baxter of Sandia National Laboratory. Minimally, 30 100 μm sized coal particles of each of the three types, namely Pittsburgh #8 (PSOC #1451), Illinois #6 (PSOC #1493) and Lower Wilcox (PSOC #1443), were selected and the surface temperature histories of these coals particles measured while irradiated with 50 ms laser pulses (12.7 MW/m^2 power flux delivered) in a nitrogen atmosphere. Average temperature histories and error bands (99% confidence) were determined in each case. These results were then modeled using the same laser flux as a fit parameter. A sphericity correction factor of 0.9 was used for all three coals [28]. Fig. 11 shows the surface temperature histories and modeling results for Pittsburgh #8 (modeled with

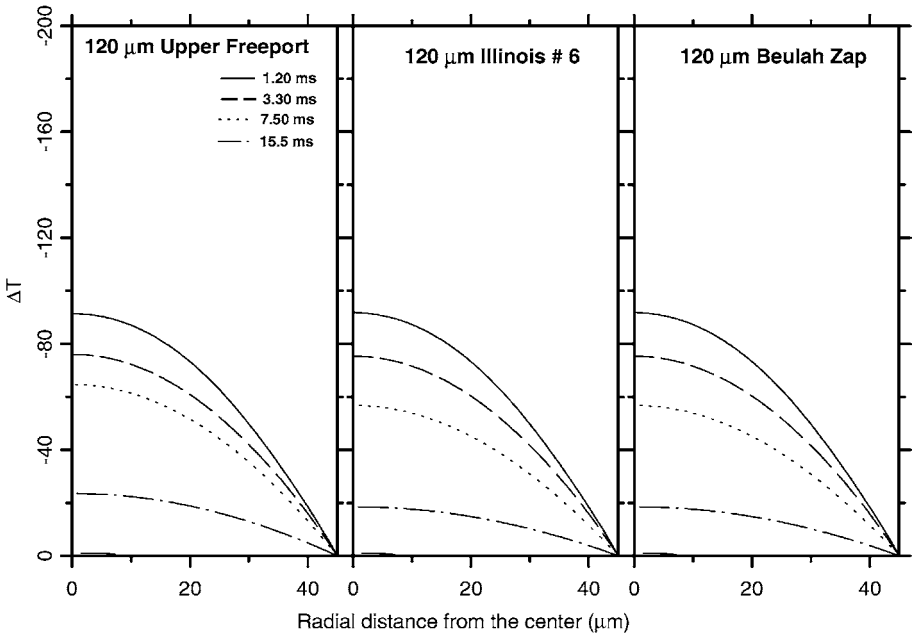

Fig. 10. Predicted intraparticle temperature gradients in the three 120 μm size coal particles. $\Delta T = T_{\text{surface}} - T_{\text{center}}$.

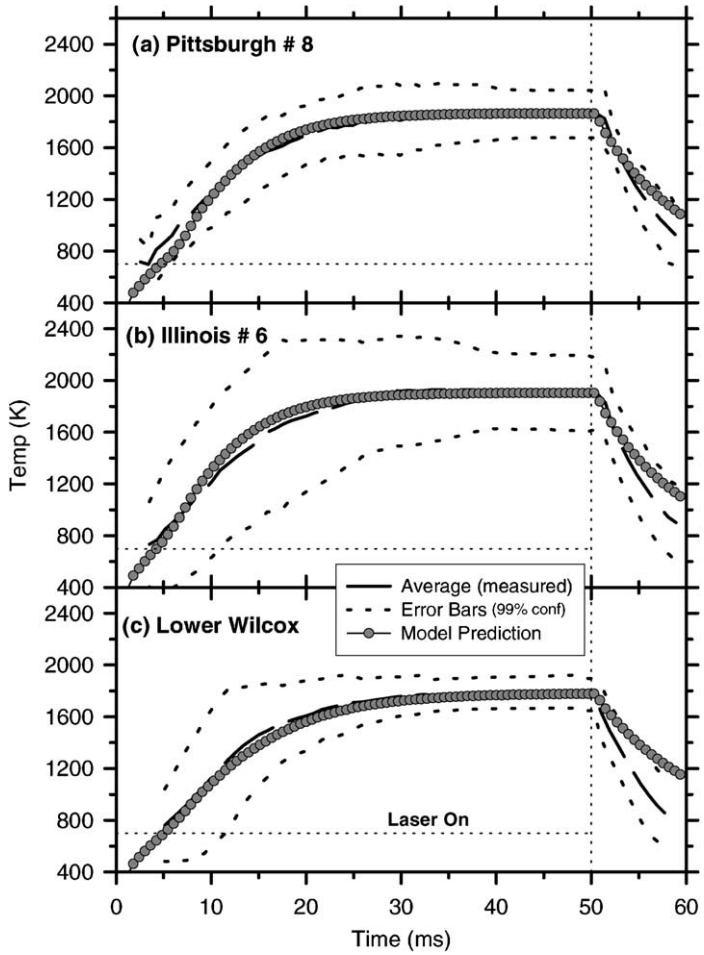

Fig. 11. Measured (average and error bars) and predicted surface temperature histories of 100 μm sized particles from three aerodynamically size-classified PSOC coals when irradiated by 50 ms CO_2 laser pulse in a nitrogen atmosphere.

3 MW/m^2, 53% wt. loss daf), Illinois #6 (modeled with 3.14 MW/m^2, 54.4% wt. loss daf) and Lower Wilcox coal (modeled with 2.8 MW/m^2, 41.8% wt. loss daf) particles, respectively. Note that these experiments were performed in a nitrogen atmosphere. Again, except for the cool-down rates (underpredicted by the model), the remaining part of the heating behavior of these coals predicted by the model lies within the error bounds.

4.7. Discrepancy in predicting cool-down rates

The cool-down rates predicted by the model are found to be lower than those observed in almost all the cases (coal ranks, particle size, ambient atmosphere, etc). The cause of this discrepancy could be many, the most likely one is the inadequacy in model assumptions. Some of these inadequacies are discussed in part 1, where a similar trend was observed for Spherocarb particles. This inadequacy becomes more pronounced in case of coal particles, which not only are non-spherical but also highly reactive. This discrepancy in cool down rates appears to be more pronounced when particles were heated in an air atmosphere and the reason for that could be char oxidation. Coal char may oxidize (following devolatilization) in air without showing any apparent change in size (shrinking core model [30]). This results in lower thermal mass of the

particle (and higher ash content) causing stored heat to dissipate quicker than the model predicts. The problem is compounded by the change in porosity. Coals have porosity in the range of 0.15–0.2, however; coal chars have porosity in the range of 0.64–0.76 [31]. Therefore, while heat-up occurs at low porosity values, cool-down process begins when coal has turned into char, i.e. at high porosity values resulting in higher probability of error (it was shown in part 1 that porosity well may be the reason for discrepancy in predicting the cool-down rates).

5. Conclusions

Clearly, heat transfer modeling of fast reacting coal particles has to deal with much more complex situation than modeling of non-reacting Spherocarb particles (as shown in part 1) under the same conditions, where the heat transport model successfully predicts the measured temperature histories. The heating behavior of the coal particle is a strong function of particle size and coal rank. Delays were observed before the start of initial heating. These delays could be attributed to the rapid increase in specific heat capacity of coals in the first 5–8 ms. The larger the particle size, the higher the temperature reached by the particles. This could be the cumulative effect of two phenomena. First of all, the larger the particle size, the lower the heat transfer coefficient and hence, the heat loss. Second, as the particle size is reduced the laser scattering increases (CO_2 laser wavelength is 10.8 μm, i.e. one order of magnitude smaller than typical particle diameters). In an air atmosphere, as particle size was increased and coal rank decreased, a temperature ''overshoot'' was observed following the initial heat-up. This could be a result of combustion of eluted products. This hypothesis was further supported by the disappearance of the observed overshoot in a nitrogen atmosphere and the fact that the use of exothermic heats of reaction by the model shows similar overshoots to those observed. A higher sphericity correction factor is required to explain the temperature histories of aerodynamic size-classified particles. This is consistent with Manozam and Maloney observations [28]. The model predicts intraparticle temperature gradients, which are maximized when the reaction rates are at their maximum. However, these gradients are smaller than the error in particle temperature history measurements. Thus, for kinetics calculation purposes use of average measured temperature histories, with error boundaries, should produce more reliable results than using predicted bulk average temperatures. This will include the errors in chemical kinetics predictions introduced by the presence of intraparticle temperature gradients.

References

[1] D.B. Anthony, J.B. Howard, AIChE J. 22 (1976) 625.
[2] P.R. Solomon, D.G. Hamblen, Chemistry of Coal Conversion, Plenum Press, New York, 1985, p. 121.
[3] L.D. Smoot, P.J. Smith, Coal Combustion and Gasification, Plenum Press, New York, 1985.
[4] W.M. Maswadeh, N.S. Arnold, W.H. McClennen, A. Tripathi, J. DuBow, H.L.C. Meuzelaar, Energy and Fuels 10 (1993) 1006–1012.
[5] W. Maswadeh, A. Tripathi, N.S. Arnold, J. DuBow, H.L.C. Meuzelaar, J. Anal. Appl. Pyrolysis 28 (1994) 55.
[6] D.J. Maloney, E.R. Monazam, S.D. Woodraff, L.D. Lawson, Combustion Flame 84 (1991) 210.
[7] J.C. Chen, M. Taniguchi, K. Narato, K. Ito, Combustion Flame 97 (1994) 107.
[8] W.M. Maswadeh, Devolatilization studies single coal particles at high heating rates, Ph.D. Thesis, University of Utah 4 (1996) 64–84.
[9] T.H. Fletcher, Combustion Sci. Technol. 63 (1989) 89.
[10] M.K. Misra, R.H. Essenhigh, Energy Fuels 2 (1988) 371.
[11] T.X. Phuoc, P. Durbetaki, J. Heat Mass Transfer 30 (11) (1987) 2231.
[12] J.T. Yang, G.G. Wang, J. Heat Transfer 112 (1990) 192.
[13] E.R. Monazam, D.J. Maloney, J. Appl. Phys. 71 (6) (1992) 2552.
[14] E.R. Monazam, D.J. Maloney, L.O. Lawson, Rev. Sci. Instrum. 60 (11) (1989) 3460.
[15] M. D'amore, L. Tognotti, A.F. Sarofim, Combustion Flame 95 (4) (1993) 374.
[16] G.M. Simmons, M. Gentry, J. Anal. Appl. Pyrolysis 10 (1986) 117.
[17] K.S. Vorres, Users handbook for the Argonne Premium Coal Sample Program, NTIS, ANL/PCSP-89/1, 1993.
[18] R.D. Bird, W.E. Stewart, E.N. Lightfoot, Transport Phenomena, Wiley Publications, 1960.
[19] W.M. Keys, M.E. Crawford, Convective Heat and Mass Transfer, 2nd Edition, McGraw-Hill Publications, 1980.
[20] L.C. Burmeister, Convective Heat Transfer, Wiley Publications, 1983.
[21] L.L. Isaccs, E. Tsafantakis, ACS Preprints Div. Fuel Chem. 32 (4) (1987) 243.
[22] L.L. Isaccs, R. Abhari, E. Tsafantakis, Energy Fuel 6 (3) (1992) 242.
[23] D. Merrick, Fuel 62 (1983) 540.
[24] D. Merrick, Fuel 62 (1983) 547.

[25] D. Merrick, Fuel 62 (1983) 553.
[26] Users Guide for FG-DVC model, Advanced Fuel Research, 1992.
[27] R.L. Braun, A.K. Burnham, Energy Fuels 1 (1987) 153.
[28] E.R. Monazam, D.J. Maloney, in: Proceedings of the 25th Symposium (International) on Combustion, The Combustion Institute, 1994.
[29] G.S. Metcalf, W. Windig, G.R. Hill, H.L.C. Meuzelaar, Int. J. Coal Geol. 7 (1987) 245.
[30] H.S. Fogler, Elements of Chemical Reaction Engineering, 2nd Edition, Prentice-Hall, NJ, 1992.
[31] K.L. Smith, L.D. Smoot, T.H. Fletcher, R.J. Pugmire, The Structure and Reaction Processes of Coal, The Plenum Chemical Series, 1994.